Structural investigation and electronic properties of the nickel ferrite $NiFe_2O_4$: a periodic density functional theory approach

2007 J. Phys.: Condens. Matter 19 346219

(http://iopscience.iop.org/0953-8984/19/34/346219)

IOP PUBLISHING JOURNAL OF PHYSICS: CONDENSED MATTER

J. Phys.: Condens. Matter **19** (2007) 346219 (10pp) doi:10.1088/0953-8984/19/34/346219

Structural investigation and electronic properties of the nickel ferrite $NiFe_2O_4$: a periodic density functional theory approach

H Perron[1,2], T Mellier[1,2], C Domain[1], J Roques[2], E Simoni[2], R Drot[2] and H Catalette[1]

[1] EDF–R&D, Département Matériaux et Mécanique des Composants, Les Renardières, Ecuelles, F-77818 Moret-sur-Loing Cedex, France
[2] IPN Orsay UMR 8608, Université Paris-Sud Orsay, Bâtiment 100, F-91406 Orsay Cedex, France

Received 17 January 2007, in final form 14 June 2007
Published 26 July 2007
Online at stacks.iop.org/JPhysCM/19/346219

Abstract

Periodic density functional theory (DFT) calculations using plane-wave basis sets were performed in order to study the bulk of nickel ferrite $NiFe_2O_4$. The local spin density approximation (LSDA) and the generalized gradient approximation (GGA) formalism were used, and it appeared that the LSDA failed to describe the magnetic structure of this compound. However, the GGA formalism gave reliable results in good agreement with experimental data for the lattice parameters, the electronic properties and the bulk modulus. In addition, the calculated density of states of the metallic species d block as well as their local magnetic moments were correlated to the crystal-field theory. Then, a charge deformation map was computed and, as expected from the electronegativity scale, the electron excess is localized around oxygen atoms along the bond axes. The formation energies of metallic vacancies are in good agreement with the inverse spinel structure experimentally observed.

(Some figures in this article are in colour only in the electronic version)

1. Introduction

For many years, the water chemistry in nuclear power plants has been the subject of several studies because it influences the material degradation, fuel failures and the radiation fields [1]. The control of material degradation is very important since some parts of the plants are very difficult to repair and can potentially limit the lifetime of the installation. Water purity also has effects on heat transfers and on the corrosion of the fuel cladding, which increases the risk of fuel failures. Finally, the dosimetry should be carefully controlled because the corrosion products are activated near the core of a reactor and are then released into the coolant system. Among these corrosion products, iron-based spinel-type compounds are largely present in the primary circuit of pressurized water reactors (PWRs). They can be found in solution as

activated colloids or deposited on pipe walls. In addition, these particles can also have retention properties relative to other activated species of the solution. It is thus of first importance to determine the physical and chemical properties of these compounds in order to minimize the dosimetry within the PWR coolant system. For this purpose, experimental studies are performed to understand and model the transport, deposition and metal ion sorption properties of these corrosion products. Furthermore, due to its technological applications as a functional material, nickel ferrite has been the subject of several experimental studies dealing with the magnetic and optical properties of nanosized particles and their synthesis techniques [5–10], ultrathin films [11] or substituted powders [12, 13].

The use of atomic-scale modelling can thus provide support to the experimental investigations by bringing complementary insights to the study of these corrosion products. In addition, from a theoretical point of view, many studies have been performed on several spinel compounds but, to our knowledge, only a few directly concern nickel ferrite [2–4].

This paper deals with the theoretical study of the bulk nickel ferrite, $NiFe_2O_4$, which mainly comes from the steam generator oxidation. In this work, periodic density functional theory (DFT) calculations were performed to optimize the lattice equilibrium parameters, the bulk modulus and the electronic structure, which were compared to experimental data. These first calculations were performed in order to determine if DFT calculations can correctly describe this complex crystalline structure in order to further build accurate surface models to study the interaction of water and ions containing radionuclides with selected crystal faces in further calculations. Such studies are of great interest to understand and control the dosimetry in the primary circuit of PWRs [14].

2. Computational details

All calculations were performed in periodic DFT using the Vienna *ab initio* simulation package VASP 4.6 [15–18]. The electronic density was optimized with the local spin density approximation (LSDA) as well as the generalized gradient approximation (GGA) as defined by Perdew and Wang [19, 20]. All atoms were described with pseudopotentials taken from the VASP library, developed on plane-wave basis sets generated with the projector-augmented-wave (PAW) method [21] and parameterized for each formalism (LSDA and GGA). These pseudopotentials are known to give slightly more accurate results than the classical ultra-soft pseudopotentials (USPPs) on magnetic systems [22]. Nickel atoms were described with ten valence electrons ($4s^2 3d^8$), iron with eight ($4s^2 3d^6$) and oxygen with six ($2s^2 2p^4$). Magnetic effects were taken into account by performing spin-polarized calculations. The Brillouin zone was integrated using different k-point sets generated with the Monkhorst–Pack method [23] centred at the Γ point with an optimized 350 eV energy cutoff. Full bulk relaxations, with atomic positions and cell (volume and shape) able to relax, were together performed using the conjugate gradient algorithm. The density of states (DOS) calculations were performed at the equilibrium volume with a $7 \times 7 \times 7$ k-point grid using the tetrahedron method with Blöchl corrections for a better accuracy [24]. The atomic radii used were the recommended ones for the pseudopotentials used in this study: 1.286 Å for Ni atoms, 1.302 Å for Fe and 0.900 Å for O. For all energy comparisons between structures, a positive value will be considered as unfavourable.

3. Results

The spinel structure is based on a face-centred cubic (fcc) unit cell of anions O^{2-} with the general formula AB_2O_4, where A and B are divalent (A^{2+}) and trivalent (B^{3+}) cations, respectively. In the normal spinel structure, the A^{2+} cations occupy 1/8 of the fcc tetrahedral

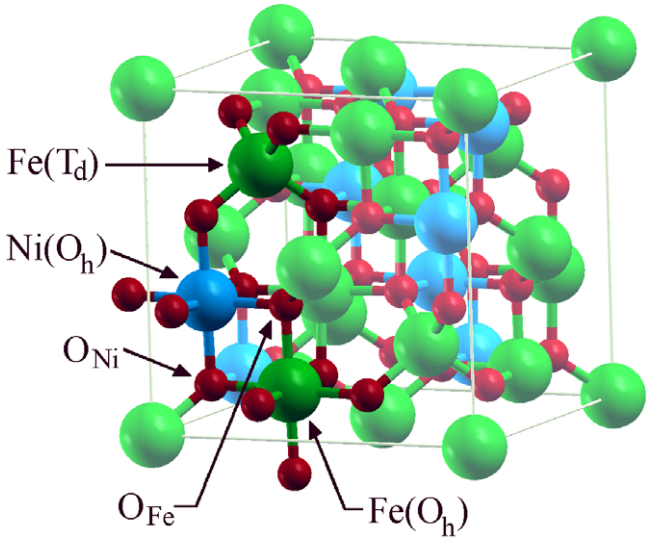

Figure 1. $NiFe_2O_4$ inverse spinel unit cell. Oxygen atoms have been added in order to complete the $Ni(O_h)$ and $Fe(O_h)$ first coordination shell. Ni atoms are shown in blue, Fe ones in green and O atoms in red.

sites (T_d) while the B^{3+} occupy 16 of the 32 available octahedral sites (O_h). An inverse spinel structure is also observed in which the B^{3+} cations are equally distributed between octahedral and tetrahedral sites while the A^{2+} cations occupy the other half of the octahedral sites. In this case, the unit cell is eightfold relative to the normal spinel one. These two structures can be written as $[A]_X[B_2]_YO_4$ and $[B]_X[AB]_YO_4$, where X and Y denote T_d and O_h sites, for the normal and inverse spinel structure, respectively.

The nickel ferrite $NiFe_2O_4$ (see figure 1) adopts an inverse spinel structure with Ni^{2+} in octahedral sites, labelled $Ni(O_h)$, and Fe^{3+} equally distributed between octahedral ($Fe(O_h)$) and tetrahedral sites ($Fe(T_d)$) of the O^{2-} fcc cell. The complete structure crystallizes in a cubic system O_h^7 space group 227; oxygen atoms occupy the 32e positions, $Fe(T_d)$ atoms occupy the 8a ones and the $Ni(O_h)$ and $Fe(O_h)$ atoms are distributed on the 16d positions, using Wyckoff notations [25]. Lattice parameters have been determined by x-ray diffraction: $a = 8.35$ Å and internal relaxation parameter $u = 0.38$ [26, 27]. The cubic unit cell thus contains 56 atoms, of which 24 are magnetic transition metals. Looking at the magnetic properties, this compound is ferrimagnetic, and the resulting magnetic moment was measured at 1.5–2.4 μ_B [12, 27]. In this structure, oxygen atoms are surrounded by four metallic cations in a pseudo-tetrahedral environment. Two oxygen species are present in the volume: the first one, denoted O_{Fe}, is surrounded by three Fe atoms (two in O_h sites and one in a T_d site) and one Ni atom; the second one, denoted O_{Ni}, is surrounded by two Fe atoms (one in an O_h site and one in a T_d site) and two Ni ones. All oxygen atoms are thus linked to three metallic cations in O_h sites and one in a T_d site.

Several calculations were performed considering LSDA and GGA formalisms in order to determine if the DFT can correctly describe the structure. In this way, both normal and inverse spinel structure with all the possible initial spin arrangements were thus investigated. From the crystal-field theory, the spin arrangement for each metallic species can be determined: the Fe^{3+} are formally d^5 and, in octahedral and tetrahedral environments (see figure 2) they can adopt a high-spin (HS) configuration; in contrast, a low-spin (LS) configuration can also be observed.

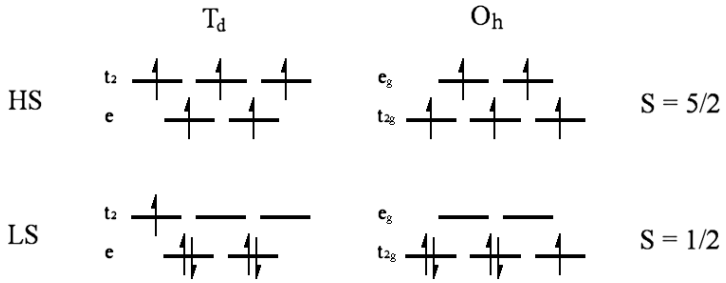

Figure 2. The d block of the Fe^{3+} cations in T_d and O_h environments with low-/high-spin (LS/HS) configurations from the crystal-field theory.

Table 1. The different possible spin arrangements for the normal ($Ni(T_d)/Fe(O_h)$) and the inverse ($Ni(O_h)/Fe(T_d)/Fe(O_h)$) spinel structure.

Normal	$Fe(O_h)\uparrow$	$Fe(O_h)\downarrow$
$Ni(T_d)\uparrow$	$\uparrow\uparrow$	$\uparrow\downarrow$
$Ni(T_d)\downarrow$	$\downarrow\uparrow$	$\downarrow\downarrow$
Inverse	**Fe(Td) ↑ /Fe(Oh) ↑**	**Fe(Td) ↓ /Fe(Oh) ↑**
$Ni(O_h)\uparrow$	$\uparrow\uparrow\uparrow$ (**1**)	$\uparrow\downarrow\uparrow$ (**4**)
$Ni(O_h)\downarrow$	$\downarrow\uparrow\uparrow$ (**2**)	$\downarrow\downarrow\uparrow$ (**3**)

This differentiation does not appear for Ni^{2+} atoms, which have a d^8 electronic configuration, leading to two unpaired electrons in the e_g or the t_2 level for O_h and T_d symmetry, respectively. The nickel ferrite crystal is composed of two magnetic sublattices [28]. The first contains all the octahedral cations $Fe(O_h)$ and $Ni(O_h)$ in a ferromagnetic arrangement with formal magnetic moments of 5 μ_B (d^5) and 2 μ_B (d^8), respectively (see figure 2). The second contains all the $Fe(T_d)$ with parallel formal magnetic moment of 5 μ_B (d^5). These two sublattices are anti-parallel, and the calculated resulting magnetic moment for the whole structure is 2 μ_B, in good agreement with the experimental range. Nevertheless, since all metallic species have initial magnetic moment, careful attention is required to take into account each possible electronic arrangement.

In the following, we will only pay attention to the atomic total spin arrangement and no longer to the detailed valence electronic structure. For each metallic species, only the resulting local magnetic moment will be considered, and this will be globally up (↑) or down (↓). For the normal spinel structure, two initial spin configurations can be considered: a ferromagnetic arrangement in which all the metallic atom magnetic moments are parallel (↑ and ↑ for $Ni(T_d)$ and $Fe(O_h)$, respectively); and a ferrimagnetic one in which the Fe^{3+} and Ni^{2+} magnetic moments are anti-parallel (↑ and ↓ for $Ni(T_d)$ and $Fe(O_h)$, respectively) (see table 1). For the inverse spinel structure, since Fe atoms are present in two environments (O_h and T_d), these two species are different and have then been treated separately. Consequently, more initial total spin arrangements have been considered, as summarized in table 1. The spin structure (**1**) is ferromagnetic and the three other structures are ferrimagnetic. Using these notations, for the experimentally observed structure, the magnetic moment arrangement is ↑↓↑ (**4**) for $Ni(O_h)/Fe(T_d)/Fe(O_h)$, respectively. In this structure, $Fe(T_d)$ and $Fe(O_h)$ are anti-parallel and, thus, in a first approximation, it can be considered that their overall magnetic moments are

Table 2. Optimized bulk parameters for normal and inverse spinel structure from GGA calculations with a $2 \times 2 \times 2$ k-point grid (exp. [11, 24, 25]: $a = 8.35$ Å, $u = 0.38$, $1.5 < \mu_{tot} < 2.4$ μ_B). Non magn. = non magnetic. The most stable structures and experimental data are shown in bold.

Structure	Initial spins	a (Å)	u	μ_{tot} (μ_B)	ΔE (eV/at.)[a]	Final spins[b]
Normal	**Ferro.**↑↑	**8.12**	**0.39**	**4.0**	**+0.05**	**+1.08/+1.31**
	Ferri. ↑↓	8.14	0.39	3.2	+0.07	−0.69/+1.92
	Non magn.	8.09	0.39			
Inverse	(**1**) ↑↑↑	8.22	0.38	4.0	+0.04	(**2**) −1.11/+3.51/+1.37
	(**2**) ↓↑↑	8.22	0.38	4.0	+0.04	(**2**) −1.11 / +3.51/+1.37
	(**3**) ↓↓↑	8.35	0.38	2.0	+ 0.05	(**3**) −1.43/−3.58/+3.51
	(**4**) ↑↓↑	**8.32**	**0.38**	**2.0**	**0.00**	(**4**) **+1.33/−3.40/+3.70**
	Non magn.	8.08	0.38			
Exp.	↑↓↑	**8.35**	**0.38**	**1.5–2.4**		

[a] The most stable structure is taken as a reference and a positive value is considered as unfavourable.
[b] Normal: $Ni(T_d)/Fe(O_h)$ and inverse: $Ni(O_h)/Fe(T_d)/Fe(O_h)$.

cancelled. The resulting magnetic field of nickel ferrite is thus mainly due to $Ni(O_h)$ atoms. In these simulations, all the local magnetic moments were able to relax and could thus switch between up/down and HS/LS spins. Non-spin-polarized calculations have also been performed in order to evaluate spin effects on the equilibrium structure.

3.1. Lattice parameters

The first calculations were performed using the local spin density approximation (LSDA). It appeared rapidly that this formalism was not appropriate in this case to properly describe this magnetic structure. The optimized lattice parameter was calculated at 7.92 Å and the metallic cations adopt a ferromagnetic structure with a large resulting magnetic moment of 4 μ_B. In addition, the normal spinel structure was calculated to be 3.03 eV more stable than the inverse one.

The same starting points as for LSDA calculations were used and optimized; results are summarized in table 2. Increasing k-point meshes were used in order to investigate the effects of the Brillouin zone sampling on relative structure energies and equilibrium parameters. The first calculations were performed using a $2 \times 2 \times 2$ k-point grid (see table 2). Regarding the results obtained for the normal spinel, the ferromagnetic structure has been characterized with low spin on metallic atoms ($\mu(Ni(T_d)) = +1.08$ μ_B and $\mu(Fe(O_h)) = +1.31$ μ_B) while the resulting magnetic moment on the oxygen ones is smaller (around $+0.1$ μ_B). For the normal ferrimagnetic spinel, a low-spin structure was also obtained with local magnetic moments of ≈ -0.69 and $\approx +1.92$ μ_B for $Ni(T_d)$ and $Fe(O_h)$, respectively.

For the inverse spinel structure, three of the four initial spin arrangements have been characterized. For the two structures where the $Fe(O_h)$ and $Fe(T_d)$ atoms are anti-parallel, (**3**) and (**4**), the lattice parameters are close to the experimental ones. In contrast, for the two others, (**1**) and (**2**), where all Fe atom spins are parallel, the lattice parameter a is shorter by about 0.1 Å. Moreover, the ferrimagnetic HS inverse structure (**4**) was found as the energetically most favourable one as observed experimentally. The local magnetic moments on the atoms are $+1.33/-3.40/+3.70/+0.10$ μ_B for $Ni(O_h)/Fe(T_d)/Fe(O_h)/O$, respectively. The non-magnetic structures have shorter lattice parameters than the magnetic ones and the normal spinel was found to be more stable than the inverse one.

In order to determine if these structures were converged, a $3 \times 3 \times 3$ k-point grid was also used with all the previous structures. No significant differences were detected and additional calculations with $4 \times 4 \times 4$ and $5 \times 5 \times 5$ k-point grids were performed only on the most

Table 3. Optimized lattice parameters and calculated bulk modulus as a function of the k-point sampling from GGA calculations on the (4) structure.

k-point sampling	a (Å)	u	μ_{tot} (μ_B)	Local magnetic moment (μ_B)[a]	B (GPa)
$2 \times 2 \times 2$	8.32	0.38	2.0	+1.33/−3.40/+3.70/+0.10	182
$3 \times 3 \times 3$	8.32	0.38	2.0	+1.34/−3.40/+3.70/+0.10	179
$4 \times 4 \times 4$	8.32	0.38	2.0	+1.34/−3.40/+3.69/+0.10	179
$5 \times 5 \times 5$	8.32	0.38	2.0	+1.34/−3.40/+3.70/+0.10	179

[a] For Ni(O_h)/Fe(T_d)/Fe(O_h)/O respectively.

stable structure (**4**) (see table 3). Regarding these optimized values, it can be considered that the structure is converged for the $2 \times 2 \times 2$ k-point mesh since the bulk lattice parameters and the local magnetic moments are almost constant.

As the same PAW pseudopotentials were used for LSDA and GGA (constructed and parameterized for both), and since they have already shown their ability on magnetic systems [22], the erroneous description must certainly come from the LSDA approximation.

Since GGA allows one to characterize the experimental structure with good lattice parameters and magnetic properties, the bulk modulus of the nickel ferrite was calculated. The bulk modulus measures the response in pressure, or resistance to a uniform compression or dilatation, due to a change in the volume relative to the equilibrium one:

$$B = -V\frac{\partial P}{\partial V} = V\frac{\partial^2 E}{\partial V^2}, \tag{1}$$

where E is the total energy of the supercell as a function of its volume V, P is the pressure and B the bulk modulus evaluated at the minimum of E. The equilibrium lattice parameters obtained with different sets of k-points were uniformly compressed or dilated by 0.5, 1.0 and 1.5%. A quadratic regression was used with the computed energies in order to calculate the bulk modulus of nickel ferrite as a function of the k-point sampling (see table 3). Unfortunately, to our knowledge, no experimental value is available in the literature, but it is experimentally known that spinel-type compounds have bulk moduli around 180–200 GPa [29]. The value calculated with the $2 \times 2 \times 2$ k-point grid (182 GPa) is in agreement with this range. The computation of this physical property is an additional result which validates the methodology.

3.2. Electronic structure

The partial densities of states for each atomic species were then studied. These allow one to analyse the electronic structure of the different species. For oxygen atoms, the up and down DOSs are nearly symmetrical, leading to a small local magnetic moment of $+0.10$ μ_B, as previously mentioned. For metallic species, only the d band was considered because it is the major part of the total density of states around the Fermi level. For the three metallic species, Ni(O_h), Fe(T_d) and Fe(O_h), a correlation with the d-block structures from the present calculations and the crystal-field theory presented in figure 2 was done. These qualitative identifications were established in order to make a comparison with the calculated local magnetic moments. These spectra are represented in figure 3. For Ni(O_h) all the up DOS is located before the Fermi level and is thus populated, while for the down DOS, only the T_{2g} band is occupied. This electronic structure leads to a calculated local magnetic moment of $+1.34$ μ_B on these atoms in agreement with the d^8 configuration expected from the crystal-field theory. Then, for Fe(T_d) atoms, all the down DOS and the E up band are below the Fermi level. The corresponding magnetic moment is calculated at -3.40 μ_B which correlates with a high-spin configuration and the d^5 structure of the crystal field theory (see figure 2). Finally,

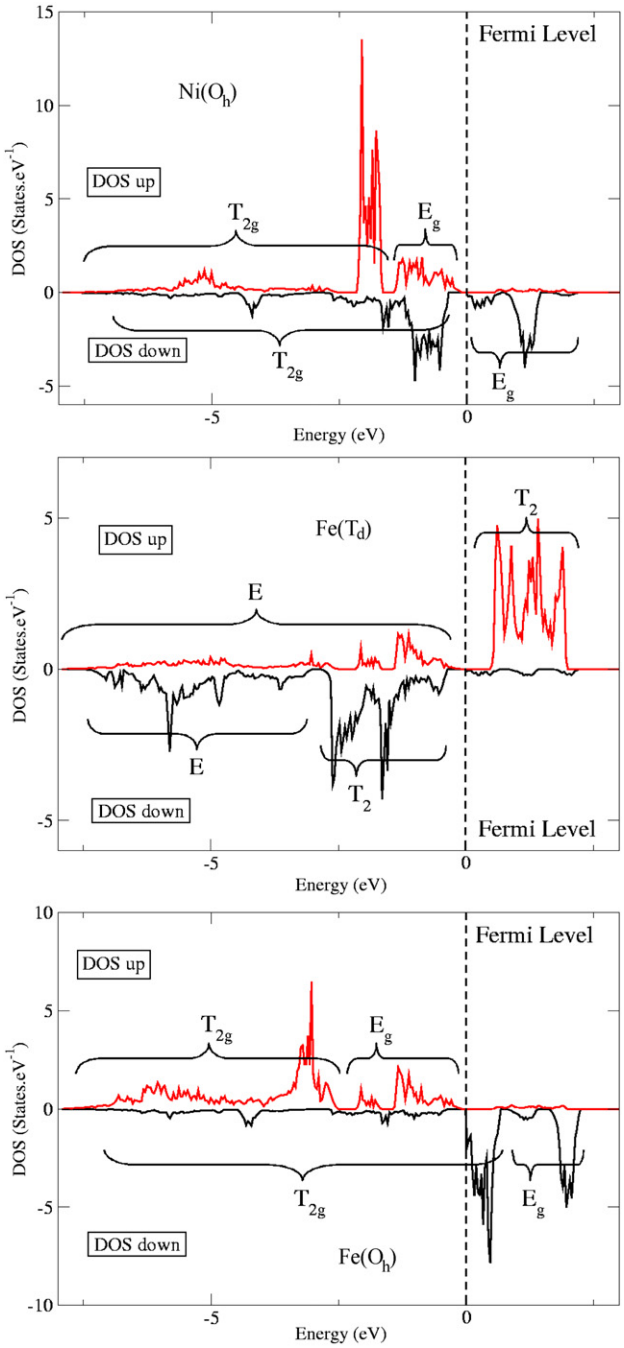

Figure 3. Partial densities of states of $Ni(O_h)$, $Fe(T_d)$ and $Fe(O_h)$ atoms, respectively.

for $Fe(O_h)$ atoms, all the up DOS is occupied as well as a small part of the down T_{2g} band. The resulting magnetic moment is $+3.70\ \mu_B$, which reveals that these atoms adopt a high-spin structure (see figure 2).

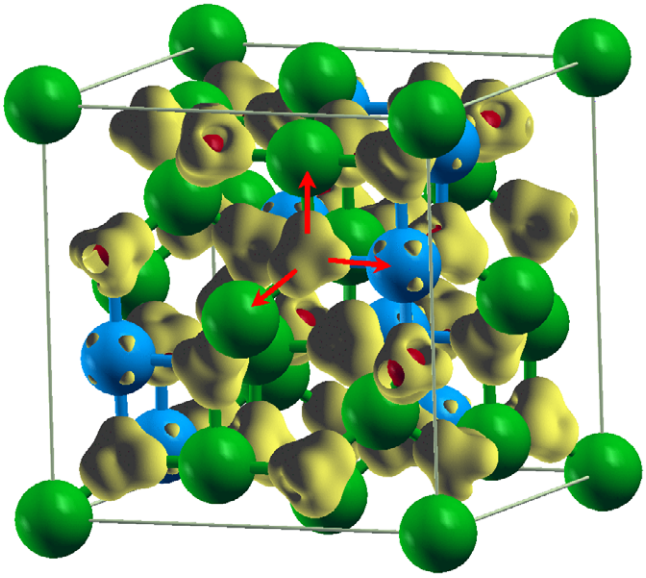

Figure 4. Charge deformation map from the equilibrium structure of $NiFe_2O_4$. The isosurface represents an excess of 0.1 electron per $Å^3$.

Table 4. Vacancy formation energies in direct and inverse spinel structures (in eV).

	$Ni(T_d)$	$Ni(O_h)$	$Fe(T_d)$	$Fe(O_h)$
Normal	0.52			1.56
Inverse		1.12	3.81	2.71

To complete this study, a qualitative investigation of the electronic transfers was performed using a charge deformation map that was computed by subtracting the charge density of each isolated atom to the spinel total one (see figure 4). This map shows the deformation of the electronic structure relative to the ideal case where all atoms are isolated and spherical. As expected, an electron excess is located on the oxygen atoms, which is in agreement with the fact that metallic atoms are oxidized while oxygen ones are reduced. This is directly linked to the relative electronegativities of these different species: 1.8 for Ni and Fe and 3.5 for O from the Pauling scale. In addition, these transfers take place along the bond axes, as suggested by the deformation of the isosurface (see red arrows on figure 4). The charge transfer is more located along the four metal–oxygen bonds, which correlates with the oxygen anions' pseudo-tetrahedral environment. A similar analysis can be done for charge defects, which are located on the metallic cations, with lobes along the bond axes reporting their octahedral and tetrahedral local symmetries.

3.3. Vacancies

Finally, metallic vacancies were introduced in both inverse and normal structures. The formation energies of these vacancies (see table 4) were calculated using the following equation:

$$E_V = E_{cell}^{V_M} + E_{ref}^{M} - E_{cell}, \tag{2}$$

where E_V is the vacancy formation energy, $E_{cell}^{V_M}$ is the total energy of the spinel unit cell with a vacancy V of a metallic cation M, E_{ref}^{M} is the reference energy of one M atom obtained from the pure crystal (fcc for Ni and bcc for Fe) and E_{cell} is the total energy of the spinel unit cell without vacancy.

These energies should report the relative stabilities between the normal and inverse structures. Fe vacancy formation energies are always larger than Ni ones, which shows that the Fe–O bonds are stronger than the Ni–O ones. Regarding the formation energies of $V_{Ni(T_d)}$ (0.52 eV) and $V_{Ni(O_h)}$ (1.12 eV) in the normal and inverse structures, respectively, it can be concluded that the Ni atoms are more stabilized in the inverse structure (by 0.60 eV). In addition, for Fe, the $V_{Fe(O_h)}$ formation energies increase also between the normal (1.56 eV) and the inverse (2.71 eV) structures. Moreover, the larger vacancy formation energy is observed for the $Fe(T_d)$ vacancy in the inverse spinel (3.81 eV). All these evolutions are consistent with the fact that the inverse structure is more stable than the normal one, as calculated above and as expected from the experimental observations on $NiFe_2O_4$.

4. Conclusion

The bulk of nickel ferrite $NiFe_2O_4$ has been studied using periodic DFT calculations. It appears that the local spin density approximation (LSDA) is not appropriate to correctly describe the magnetic structure of this spinel structure. However, the generalized gradient approximation (GGA) leads to results that are in good agreement with experimental data in terms of lattice parameters and magnetic moment. The bulk modulus was computed and the calculated value (≈180 GPa) is in agreement with the experimental 180–200 GPa range for spinel-type compounds. Regarding the effects of an increase in the k-point mesh, it appears that a $2 \times 2 \times 2$ grid is sufficient to get converged bulk parameters and local magnetic moments. Furthermore, the partial densities of states were computed within the GGA formalism, allowing a detailed knowledge of the electronic structure. Using the crystal-field theory, the valence electrons were attributed to the different bands of the metallic species d block and the corresponding calculated local magnetic moments were found to be in agreement. Finally, the charge transfers were qualitatively studied with the computed charge deformation map, and as expected from the Pauling electronegativity scale, an electron excess, which is more developed along the bond axes, was found around oxygen atoms. Finally, metallic vacancies were introduced in order to complete the study of the relative stability between the normal and the inverse spinel structures of $NiFe_2O_4$. All formation energies are larger for the inverse spinel relative to the normal one leading to a greater stability of the inverse structure.

This study was performed with the aim of finding an accurate computational method to describe this magnetic spinel compound in order to further investigate, on well-defined crystal faces, the retention properties relative to ionic species containing radionuclides that can be found in the coolant systems of nuclear power plants.

Acknowledgment

All calculations were performed using the CEA CCRT supercomputers, in the framework of an EDF–CEA partnership.

References

[1] Fruzzetti K and Wood C J 2006 *Proc. Int. Conf. on Water Chemistry of Nuclear Reactor Systems (Jeju Island, Korea, 23–26 October 2006)*

[2] Zuo X, Yan S, Barbiellini B, Harris V G and Vittoria C 2006 *J. Magn. Magn. Mater.* **303** e432

[3] Kodama R H and Berkowitz A E 1999 *Phys. Rev.* B **59** 6321
[4] Bercoff P G and Bertorello H R 1997 *J. Magn. Magn. Mater.* **169** 314
[5] Kodama R H, Berkowitz A E, McNiff E J Jr and Foner S 1996 *Phys. Rev. Lett.* **77** 394
[6] Nathani H, Gubbala S and Misra R D K 2005 *Mater. Sci. Eng.* B **121** 126
[7] Chinnasamy C N, Narayanasamy A, Ponpandian N, Chattopadhyay K, Shinoba K, Jeyadevan B, Tohji K and Nakatsuka K 2001 *Phys. Rev.* B **63** 184108
[8] Huang X and Chen Z 2004 *J. Magn. Magn. Mater.* **280** 37
[9] Cheng Y, Zheng Y, Wang Y, Bao F and Qin Y 2005 *J. Solid State Chem.* **178** 2394
[10] Mohallem N D S and Seara L M 2003 *Appl. Surf. Sci.* **214** 143
[11] Lüders U, Bibes M, Bobo J F, Cantoni M, Bertacco R and Fontcuberta J 2005 *Phys. Rev.* B **71** 134419
[12] Bhosale A G and Chougule B K 2006 *Mater. Chem. Phys.* **97** 273
[13] Hwon L S, Yoon S J, Lee G J, Kim H S, Yo C H, Ahn K, Lee D H and Kim K H 1999 *Mater. Chem. Phys.* **61** 147
[14] Perron H 2007 *PhD Thesis* University of Paris 11, France
[15] Kresse G and Hafner J 1993 *Phys. Rev.* B **47** 558
[16] Kresse G and Hafner J 1994 *Phys. Rev.* B **49** 14251
[17] Kresse G and Furthmüller J 1996 *Comput. Mater. Sci.* **6** 15
[18] Kresse G and Furthmüller J 1996 *Phys. Rev.* B **54** 11169
[19] Perdew J P and Wang Y 1992 *Phys. Rev.* B **45** 13244
[20] Perdew J P, Chevary J A, Vosko S H, Jackson K A, Pederson M R, Singh D J and Fiolhais C 1992 *Phys. Rev.* B **46** 6671
[21] Blöchl P E 1994 *Phys. Rev.* B **50** 17953
[22] Kresse G and Joubert D 1999 *Phys. Rev.* B **59** 1758
[23] Monkhorst H J and Pack J D 1976 *Phys. Rev.* B **13** 5188
[24] Blöchl P E, Jepsen O and Andersen O K 1994 *Phys. Rev.* B **49** 16223
[25] Wyckoff R 1964 *Crystal Structures* 2nd edn, vol 1 (New York: Interscience)
[26] Lee S H, Yoon S J, Lee G J, Kim H S, Yo C H, Ahn K, Lee D H and Kim K H 1999 *Mater. Chem. Phys.* **61** 147
[27] West A R 1999 *Basic Solid State Chemistry* 2nd edn (Chichester: Wiley) p 388
[28] Lüders U, Bibes M, Bobo J-F, Cantoni M, Bertacco R and Fontcuberta J 2005 *Phys. Rev.* B **71** 134419
[29] Recio J M, Franco R, Martín Pendás A, Blanco M A, Puyeo L and Pandey R 2001 *Phys. Rev.* B **63** 184101